Cerebral Cortex December 2013;23:2790–2802
doi:10.1093/cercor/bhs210
Advance Access publication August 31, 2012

Axo-Dendritic Overlap and Laminar Projection Can Explain Interneuron Connectivity to Pyramidal Cells

Adam M. Packer, Daniel J. McConnell, Elodie Fino and Rafael Yuste

HHMI, Department of Biological Sciences, Columbia University, New York, NY 10027, USA

Address correspondence to Adam Packer, Wolfson Institute for Biomedical Research, Cruciform Building, University College London, Gower Street, London WC1E 6BT, UK. Email: adampacker@gmail.com.

Neocortical GABAergic interneurons have important roles in the normal and pathological states of the circuit. Recent work has revealed that somatostatin-positive (SOM) and parvalbumin-positive (PV) interneurons connect promiscuously to pyramidal cells (PCs). We investigated whether Peters' rule, that is, the spatial overlap of axons and dendrites, could explain this unspecific connectivity. We reconstructed the morphologies of P11–17 mouse SOM and PV interneurons and their PC targets, and performed Monte Carlo simulations to build maps of predicted connectivity based on Peters' rule. We then compared the predicted with the real connectivity maps, measured with 2-photon uncaging experiments, and found no statistical differences between them in the probability of connection as a function of distance and in the spatial structure of the maps. Finally, using reconstructions of connected SOM-PCs and PV-PCs, we investigated the subcellular targeting specificity, by analyzing the postsynaptic position of the contacts, and found that their spatial distributions match the distribution of postsynaptic PC surface area, in agreement with Peters' rule. Thus, the spatial profile of the connectivity maps and even the postsynaptic position of interneuron contacts could result from the mere overlap of axonal and dendritic arborizations and their laminar projections patterns.

Keywords: GABA, microcircuit, Peters' rule, synapse

Introduction

The neocortical GABAergic interneurons are a fascinating group of cells with large morphological, physiological, and molecular diversity (Fairen et al. 1984; Somogyi et al. 1998; Ascoli et al. 2008). Although their function is not well understood, they are altered in a variety of diseases, including epilepsy and schizophrenia (Prince and Wilder 1967; Lewis et al. 2011), and they could be necessary for maintaining the operating regime of the excitatory cells, perhaps controlling their temporal firing patterns (Buzsaki and Chrobak 1995; Monyer and Markram 2004; Kapfer et al. 2007).

To better understand the function of neocortical interneurons, it could be important to map their synaptic connectivity. Recently, the connectivity of 2 major subtypes of neocortical interneurons, somatostatin-positive (SOM), and parvalbumin-positive (PV) interneurons, was investigated using 2-photon RuBi-Glutamate uncaging and multiple patch-clamp recordings in brain slices (Fino and Yuste 2011; Packer and Yuste 2011). Those experiments revealed dense and unspecific connections from SOM and PV interneurons to pyramidal cells (PCs) in upper and lower layers of the mouse frontal and somatosensory cortex. But in apparent contradiction with this nonspecific targeting of postsynaptic PCs by interneurons, there is ample evidence that interneurons selectively target different subcellular compartments that differ among interneuron subtypes (Buhl et al. 1994; Somogyi et al. 1998). This targeting can be extremely specific, as in the case of chandelier cells, which solely contact axon initial segments (Somogyi 1977) or less so, as in the case of SOM and PV interneurons, which mostly contact dendritic or somatic compartments, respectively (Fairen et al. 1984; Kawaguchi and Kubota 1997; Di Cristo et al. 2004; Wang et al. 2004). The subcellular specificity of this targeting could arise from the presence of particular postsynaptic molecules in selective regions of the postsynaptic cell (Ango et al. 2004, 2008; Di Cristo et al. 2004; Huang et al. 2007).

We were puzzled by this apparent discrepancy, where on the one hand interneuron axons can selectivity contact very precise subregions of their PC targets, while at the same time these same axons seem to innervate every available PCs in a highly nonselective manner. Though it is possible that independent developmental mechanisms dictate interneuron connectivity, such an explanation is less parsimonious than a single one. Motivated to find a simple explanation, we sought to better understand the mechanisms responsible for the circuit connectivity of SOM and PV interneurons, by reconstructing the morphologies of the axons, and the dendrites of their pyramidal targets, in both somatosensory and frontal mouse cortex. Because the connectivity patterns of SOM and PV interneurons appear unspecific, we tested whether the overlap of axons and dendrites, that is, Peters' rule (Peters and Feldman 1976), could explain it. For this purpose, we first performed numerical simulations to calculate the predicted connectivity maps according to Peters' rule, finding that the calculated maps very closely resemble the measured maps. We then examined the subcellular position of the interneuronal contacts onto PCs, by reconstructing pairs of connected SOM-PC and PV-PC and measuring the position of all their putative contacts. For both subtypes, the axo-dendritic and axo-somatic appositions were located in proportion to the postsynaptic surface area of the PC. Thus, differences between SOM and PV dendritic versus somatic targeting could be simply explained because SOM axons project to layer 1, which lack PC somata, whereas PV axons project to layers where most PC somata are found. Since our data were taken from P11 to 17 mice, we limit our conclusion to the juvenile postnatal developmental period.

Materials and Methods

Slice Preparation and Electrophysiology

All animal handling and experimentation was done according to the National Institutes of Health and local Institutional Animal Care and Use Committee guidelines. Somatosensory or frontal coronal slices

(350-μm thick) were prepared from GIN (Oliva et al. 2000) or G42 mice (Chattopadhyaya et al. 2004), of either sex, postnatal ages P11–17, using a Leica VT1000S or VT1200S vibratomes with ice-cold sucrose solution containing (in mM): 27 $NaHCO_3$, 1.5 NaH_2PO_4, 222 sucrose, 2.5 KCl, 3 $MgSO_4$, and 1 $CaCl_2$. Slices were incubated at 36 °C for 30 min in ACSF containing (in mM): 126 NaCl, 26 $NaHCO_3$, 1.1 NaH_2PO_4, 10 glucose, 3 KCl, 3 $MgSO_4$, and 1 $CaCl_2$. During recordings made at 32 °C, ACSF composition was similar except for the following (in mM): 2 $MgSO_4$ and 2 $CaCl_2$. All sucrose and ACSF solutions were saturated with 95% O_2 and 5% CO_2.

Whole-cell recordings were made using Multiclamp 700B amplifiers (Molecular Devices, Sunnyvale, CA, United States of America), digitized with National Instruments 6259 multichannel cards, and recorded using custom-made software using the LabView platform (National Instruments, Austin, TX, United States of America). Current-clamp recordings were performed with intracellular solution (pH 7.2) containing (in mM): 135 K-methylsulfate, 8 NaCl, 10 HEPES, 2 Mg-ATP, 0.3 Na-GTP, 7 phosphocreatine, 0.02 Alexa Fluor 594, and 10.7 biocytin. Voltage-clamp recordings were performed with intracellular solution (pH 7.3) containing (in mM): 128 cesium methanesulfonate, 10 HEPES, 10 Na-phosphocreatine, 2 $MgCl_2$, 3 $MgSO_4$, 4 Mg-ATP, 0.4 Na-GTP, 0.02 Alexa Fluor 594, and 10.7 biocytin.

Imaging and Uncaging

Data from input maps were used previously in 2 studies focused on characterizing the spatial distribution of the connectivity (Fino and Yuste 2011; Packer and Yuste 2011). Two-photon imaging and RuBi-Glutamate uncaging were performed as described in Fino et al. (2009); Fino and Yuste (2011); Packer and Yuste (2011). Briefly, images were acquired using a custom-made 2-photon laser scanning microscope based on the Olympus FV-200 system (side mounted to a BX50WI microscope with a ×40 0.8-NA or ×20 0.5-NA water-immersion objective) and a Ti:sapphire laser (Chameleon Ultra II, Coherent, >3 W, 140 fs pulses, 80 MHz repetition rate). Images were acquired at 850 or 900 nm for GFP and 800 nm for Alexa 594 with minimal power to avoid uncaging RuBi-Glutamate. An aliquot of 300 μM RuBi-Glutamate (Tocris, Ellisville, MO, United States of America) was added to the oxygenated ACSF during mapping experiments and was recirculated with a peristaltic pump (RP-1, Rainin Instruments, Oakland, CA, United States of America). All mapping experiments were conducted using the ×20 0.5-NA objective. We used custom software (Nikolenko et al. 2007) to create the complex targets around cell bodies. Each complex target, which consisted of 5 beamlets due to the diffractive optical element we used, was illuminated for 8 ms, resulting in a stimulation of 72 ms with an additional millisecond to move between targets. A Pockels cell (Conoptics, Danbury, CT, United States of America) allowed us to control power precisely over these short durations. The power at the sample ranged from 150 to 330 mW for mapping experiments. We used multiple different power levels in each mapping experiment, always testing the maximum level to ensure detecting connections from any SOM or PV interneurons, especially for PV interneurons with particularly high rheobases.

Biocytin Histochemistry and Reconstructions

At the end of an experiment, slices were fixed and kept overnight in 4% paraformaldehyde in 0.1 M phosphate buffer (PB) at 4 °C. The slices were then rinsed 3 times for 5 min per rinse on a shaker in 0.1 M PB. They were placed in 30% sucrose mixture (30 g sucrose dissolved in 50 mL ddH_20 and 50 mL 0.24 M PB) for 2 h and then frozen on dry ice in tissue freezing medium. The slices were kept overnight in a −80 °C freezer. The slices were defrosted and the tissue freezing medium was removed by three 20 min rinses in 0.1 M PB while on a shaker. The slices were kept in 1% hydrogen peroxide in 0.1 M PB for 30 min on the shaker to pretreat the tissue, then were rinsed twice in 0.02 M potassium phosphate saline (KPBS) for 20 min on the shaker. The slices were then kept overnight on the shaker in Avidin-Biotin-Peroxidase Complex. The slices were then rinsed 3 times in 0.02 M KPBS for 20 min each on the shaker. Each slice was then placed in 3,3″-diaminobenzidine (DAB, 0.7 mg/mL; 0.2 mg/mL urea hydrogen peroxide, 0.06 M Tris buffer in 0.02 M KPBS) until the slice turned light brown, then immediately transferred to 0.02 M KPBS, and finally transferred again to fresh 0.02 M KPBS after a few minutes. The stained slices were rinsed a final time in 0.02 M KPBS for 20 min on a shaker. Each slice was observed under a light microscope and then mounted onto a slide using crystal mount. Successfully filled and stained neurons were then reconstructed using Neurolucida software (MicroBrightField, Williston, VT, United States of America). The neurons were viewed with a ×100 oil objective on an Olympus IX71 inverted light microscope or an Olympus BX51 upright light microscope. The Neurolucida program projected the microscope image onto a computer drawing tablet. The neuron's processes were traced manually, while the program recorded the coordinates of the tracing to create a digital, 3-dimensional reconstruction. The user defined an initial reference point for each tracing. The *z*-coordinate was then determined by adjustment of the focus. In addition to the neuron, the pia and white matter were drawn.

Morphological Analysis

Input map data were analyzed as before (Fino and Yuste 2011; Packer and Yuste 2011). Axon and dendrite densities were calculated from the Neurolucida reconstruction using the TREES toolbox (Cuntz et al. 2010) to determine the amount of cellular process inside voxels 3, 5, or 10 μm on each side. Nearly identical results were obtained with voxels of different sizes on a subset of data:

1. S23 predicted versus observed: Voxel = 3, $R = 0.80$; voxel = 5, $R = 0.80$; voxel = 10, $R = 0.79$.
2. S5 predicted versus observed: Voxel = 3, $R = 0.83$; voxel = 5, $R = 0.83$; voxel = 10, $R = 0.83$.
3. S23 predictions versus S5 observations: Voxel = 3, $R = -0.49$; voxel = 5, $R = -0.51$; voxel = 10, $R = -0.50$.
4. S5 predictions versus S23 observations: Voxel = 3, $R = -0.12$; voxel = 5, $R = -0.12$; voxel = 10, $R = -0.12$.

Thus, voxels of 5 μm were used in the remained of the study and reported in the results. "Average neurons" were produced by simply summing the densities of each neuron of a given type together. Surface area was calculated using Neurolucida, which considers a cellular process to be an idealized cylinder.

Contacts were defined by the crossing of a presynaptic axon and postsynaptic dendrite within 1.0 μm with a visible synaptic bouton on the presynaptic axon. The cells were viewed under an Olympus BX51 upright light microscope with a ×100 oil objective and projected onto a computer screen using Neurolucida. Possible contacts were then found by finding cell overlaps using the cell reconstruction. Image stacks were taken from the location of the presynaptic bouton to the center of the postsynaptic dendrite. Contacts were accepted if the pre- and postsynaptic processes were determined to be within 1.0 μm (DeFelipe and Fairen 1982; Reyes et al. 1998; Tamas et al. 2002; Tanaka et al. 2011).

Statistical Analysis

Off-line analysis was conducted using MATLAB (Mathworks, Natick, MA, United States of America), InStat (GraphPad, La Jolla, CA, United States of America), MiniAnalysis (Synaptosoft, Decatur, GA, United States of America), and Oriana (Kovach Computing Services, Wales, UK). Additional circular statistics tests were performed with the MATLAB CircStat Toolbox (Berens 2009). All results are expressed as mean ± standard error of the mean.

Results

Spatial Profiles of Output Connectivity from PV and SOM Interneurons

To understand the mechanisms responsible for the generation of interneuron connectivity in the neocortex, we studied connections from PV and SOM interneurons to PCs. Since it

has been previously shown that these subpopulations of interneurons connect quite indiscriminately with PCs, without any apparent specificity (Fino and Yuste 2011; Packer and Yuste 2011), we first considered the hypothesis that the connections from PV and SOM neurons to PC could be determined by chance, meaning that interneuron axons make synapses with PC dendrites whenever they are in sufficiently close proximity. In this scenario, first suggested by Peters et al. (1976), the mere structural overlap of axons and dendrites determines the connectivity.

To test this hypothesis, we first collected the maps of connectivity between PV and SOM interneurons, using an optical technique to map inhibitory inputs to neurons [data previously presented in Fino and Yuste (2011); Packer and Yuste (2011)]. Specifically, in order to detect which interneurons were connected to PCs, we used 2-photon glutamate uncaging to photostimulate individual interneurons in the somatosensory and frontal cortex of acute brain slices from postnatal (P11–17) PV (G42; Chattopadhyaya et al. 2007) and SOM (GIN; Oliva et al. 2000) transgenic animals, in which specific interneuron populations express GFP. We first patched one or more PCs (Fig. 1*A*, blue arrow), bathed the slice in the photoactivatable compound RuBi-Glutamate (Fino et al. 2009), and then sequentially targeted the 2-photon laser to stimulate each interneuron in the field of view (Fig. 1*A*, circles). Connected interneurons (Fig. 1*A*, red circles) elicited large, short latency outward currents upon photostimulation when the postsynaptic PC was maintained at a holding potential of +40mV (Fig. 1*B*, top trace). Employing a "flip test" (Fino and Yuste 2011), we confirmed that such inputs were inhibitory since they did not change direction when the PC was switched to a holding potential of −40 mV. Unconnected neurons (Fig. 1*A*, gray circles) showed no response (Fig. 1*B*, bottom trace). Rare excitatory connections (Fig. 1*A*, black circles), perhaps due to inadvertent stimulation of the dendrite of the postsynaptic cell directly, or of a nearby connected excitatory neuron (Fig. 1*B*, stimulation 4), were identified as such because they changed polarity when the PC holding potential was switched around the glutamate reversal potential. Those contaminating "false positive" excitatory responses were discarded for our analysis.

Using this approach, we probed connectivity from interneurons across multiple focal planes, producing inhibitory input maps with single-cell resolution (Fig. 1*C*). We produced such maps for multiple postsynaptic neurons at one time (Fig. 1*D*), resulting in a database of connectivity from interneurons to PCs across 2 cell types (PV and SOM), 2 neocortical areas (somatosensory and frontal cortex), and 2 cortical layers (layers 2/3 and 5). Overall, we mapped the connections of 2992 interneurons to 143 PCs. We tested the connections from 1747 PV interneurons, generating 82 maps of PV connectivity: 23 in layer 2/3 frontal cortex (F2/3), 38 in layer 2/3 somatosensory cortex (S2/3), and 21 in layer 5 somatosensory cortex (S5). In addition, we tested the connections from 1245

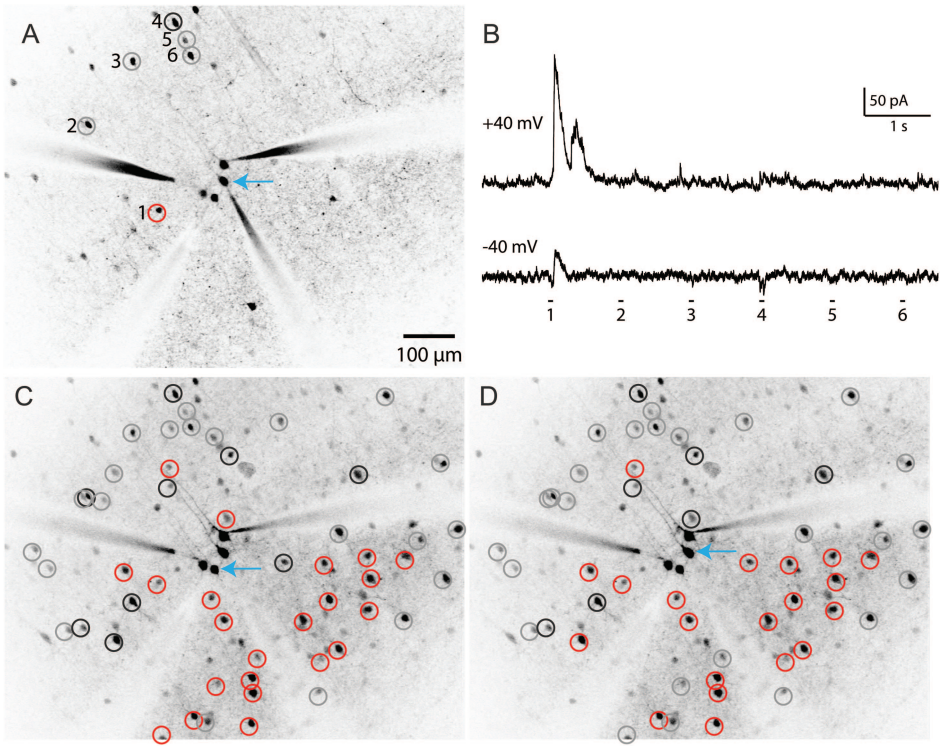

Figure 1. Mapping inputs from interneurons to pyramidal cells. (*A*) Two-photon mapping of synaptic connections from 6 PV interneurons (numbered) onto a PC (blue arrow). (*B*) PV interneurons were photostimulated with 2-photon RuBi-Glutamate uncaging as described previously (Packer and Yuste 2011). Interneurons were sequentially stimulated, while responses were recorded from the postsynaptic PC held at a membrane potential of +40 or −40 mV (upper and lower traces) to distinguish inhibitory from rare but possible excitatory inputs. Note the large, low-latency IPSCs evoked during the stimulation of interneuron 1 (red circle, left), which do not change direction around the glutamate reversal potential, indicating an inhibitory monosynaptic connection from this interneuron. All other interneurons show no response indicating a lack of synaptic connection (gray circles), while interneuron 4, on the other hand, exhibits a weak excitatory response and is labeled as false positive (black circle). (*C*) Checking all interneurons in this field of view across multiple focal planes yields an inhibitory input map for the PC indicated by the blue arrow. (*D*) Another input map for a different PC directly adjacent to the PC mapped in *C*. The other PCs patched in this field did not yield recordings of sufficient quality for mapping.

SOM interneurons, generating 61 maps of SOM connectivity in F2/3. While there was variability from map to map and across cortical areas and layers, a consistent finding was that interneurons invariably connected at high rates to PCs nearby in a nonspecific fashion. As described previously, the average connection probability was 18%, 36%, and 33% for PV interneurons (S2/3, S5, and F2/3, respectively) and 43% for SOM interneurons, but for PV interneurons located within 100 μm of the recorded PC it increased to 43%, 67%, and 75% (S2/3, S5, and F2/3, respectively) and 71% for SOM interneurons within 200 microns (Fino and Yuste 2011; Packer and Yuste 2011). Moreover, in many individual maps of both SOM and PV interneurons, every single interneuron located in the close vicinity (<100 μm) of a PC was connected to it (Fino and Yuste 2011; Packer and Yuste 2011).

Predicting Connectivity Maps of PV Interneurons from Peters' Rule

We then sought to understand the mechanisms underlying the dense synaptic connectivity maps we observed, and for the differences in the spatial connectivity patterns observed between layers (Packer and Yuste 2011). For this purpose, we considered that perhaps the arborizations of PV and SOM interneuron axons and PC dendrites alone could explain the maps. In other words, could the morphologies of the cells simply predict the spatial connectivity profiles we measured, as one would expect from Peters' rule?

To generate a morphological database for our analysis, we reconstructed PV interneurons ($n = 15$; 11 S2/3, 4 S5), SOM interneurons ($n = 5$; F2/3), and PCs ($n = 19$; 5 F2/3, 6 S2/3, 8 S5; Fig. 2; Supplementary Fig. S1), from the same cortical areas and layers from which we had measured the connectivity maps. Reconstructed interneurons exhibited very dense axonal fields, with distinct profiles for PV and SOM interneurons. PV interneurons had somata located in layers 2/3 and 5, with local axonal arbors, and often had vertical interlaminar projections (Fig. 2, middle panels; Supplementary Fig. S1). Meanwhile, SOM interneurons had distinctive Martinotti-like axonal patterns, with ascending axons that arborized in layer 1 (Fig. 2, right; Wang et al. 2004; McGarry et al. 2010). Finally, PC had somata located at different laminar positions and typical morphologies with apical dendrites that extended toward layer 1 (Fig. 2, left).

To test whether Peters' rule could explain our findings, we focused first on the PV-PC connectivity maps and used our morphological database to calculate the average axo-dendritic overlap between axons of PV interneurons and dendrites of PCs in layers S2/3 and S5. First, we computed an average morphology for each neuronal type by projecting together the densities of 8 S2/3 PV interneuron axons, 4 S5 PV interneuron axons, and 5 PC somata and dendrites (Fig. 3*A*, density computed with voxels 5 μm on each side, see Materials and Methods). Next, we multiplied the spatial profile of the average interneuron axon with the spatial profile of the average PC soma and dendrite to generate an average map of the spatial overlap of the axons and dendrites. This spatial overlap is a measure of the probability that axonal and dendritic processes occupy the same voxel in space. We then summed the spatial overlap to yield a single numerical value, which we called the axo-dendritic overlap. We then repeated this calculation, systematically offsetting the positions of the somata of the PV interneurons and PCs with the coordinates of every interneuron tested from the input maps. This calculation produced an estimate of axo-dendritic overlap for each PV-PC pair optically tested in the input maps ($n = 1266$ pairs, 709 S2/3, 557 S5).

Overlap of Axons and Dendrites Predicts Spatial Connectivity Profiles of PV Interneurons

We then compared the axo-dendritic overlap with the known spatial connectivity profiles of the PV interneurons in order to quantitatively assess to what extent the spatial features of the measured connectivity of PV interneurons could be attributed solely to the particular morphologies of their axons. We chose to analyze 2 distinct features of the connectivity maps: The probability of connection as a function of distance to the PC soma, and the spatial structure of the maps, in polar coordinates, within a given cortical territory.

We first compared the distance dependency of the PV-PC connectivity index, that is, the percentage of presynaptically connected PV interneurons in a series of Sholl-like,

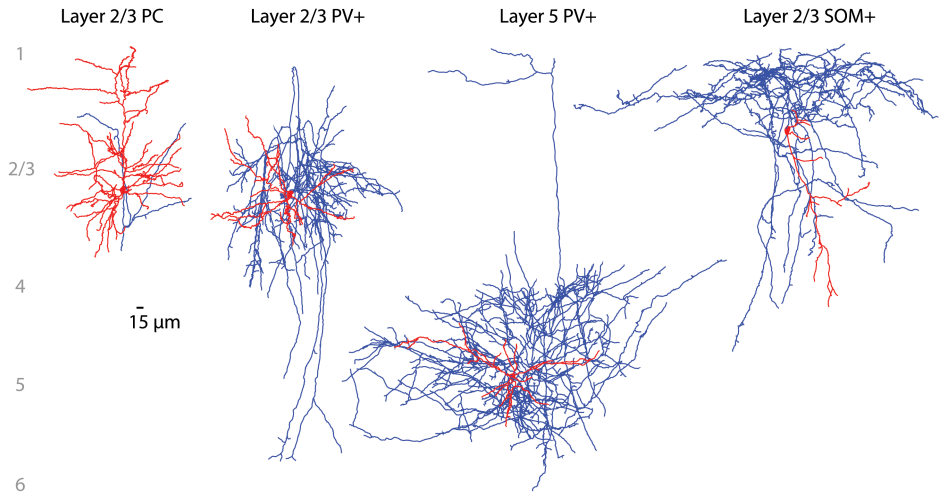

Figure 2. Anatomical reconstructions of PCs and GABAergic interneurons. Representative morphological reconstructions of a layer 2/3 PC, layer 2/3 and 5 PV interneurons, and a layer 2/3 SOM interneuron (from left to right; axons in blue, dendrites in red). Note the striking density of the interneuron axonal fields.

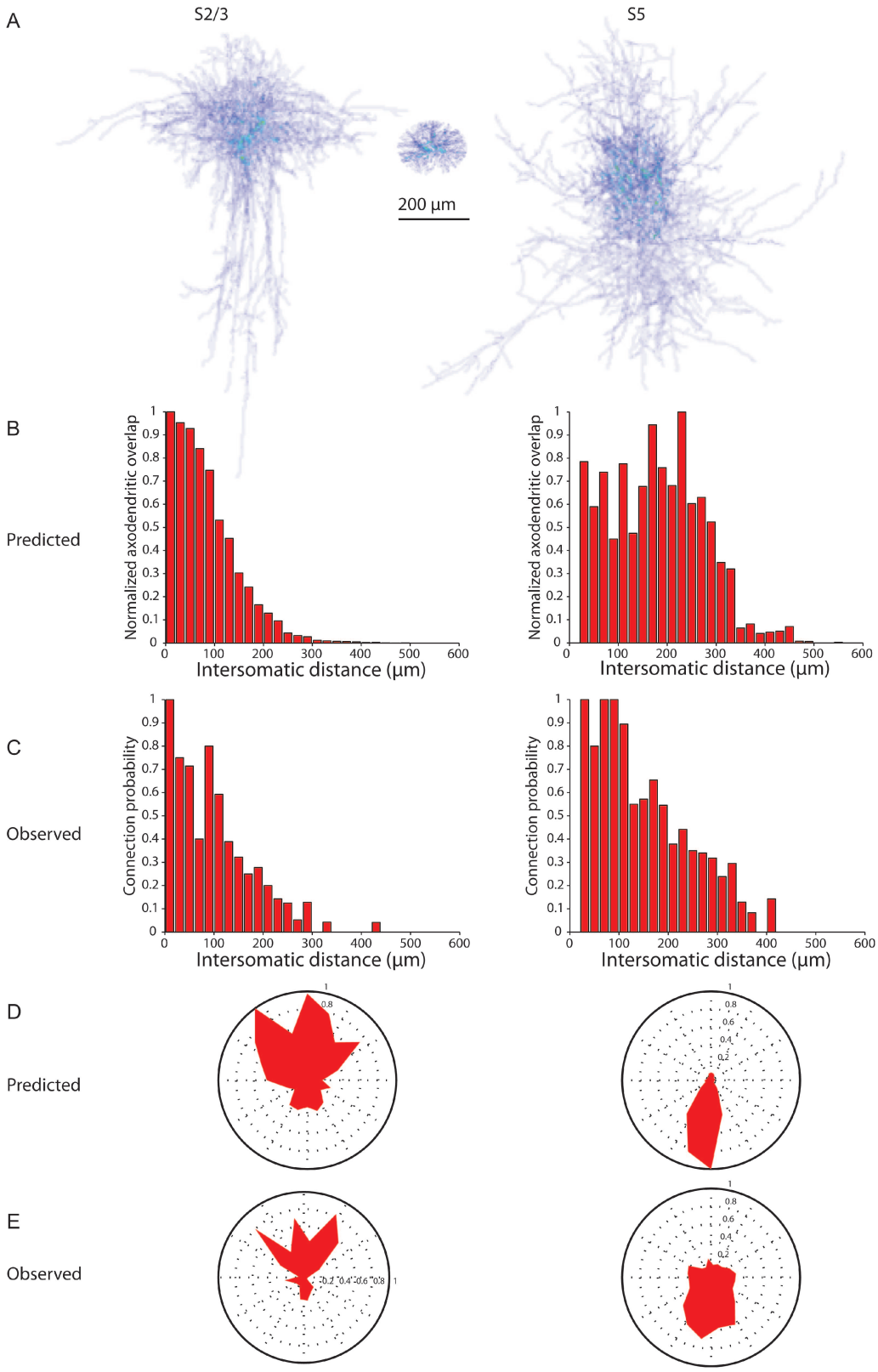

Figure 3. Axo-dendritic overlap can predict the spatial patterns of PV connectivity. (*A*) Average density of 8 somatosensory layer 2/3 PV interneuron axons (left), 5 PC cell bodies and dendrites within 100 µm (middle), and the average density of 5 somatosensory layer 5 PV interneuron axons (right) were multiplied to produce a measure of axo-dendritic overlap between axons of PV interneurons and soma and dendrites of PCs. This value was calculated using the intersomatic distances of the PV interneurons and PCs tested in the maps. (*B–E*) The amount of overlap between the axons of the layers 2/3 (left column) and layer 5 (right column) PV interneurons and the dendrites and cell bodies of the PCs predicts the observed connectivity profiles with regard to both distance (*B*, *C*) and angular distribution (*D*, *E*). The observed probability of connection was reported previously (Packer and Yuste 2011), although with different binning for the angular distribution (*E*).

sequentially larger radial spheres from a typical PC. We found that the maps of measured connectivity patterns between PV interneurons and layers 2/3 and 5 PCs were remarkably similar to calculated maps generated by axo-dendritic overlap (Fig. 3*B*,*C*). Specifically, at every intersomatic distance, the axo-dendritic overlap calculated was not significantly different from the measured connection probability ($R = 0.95$, $P < 0.0001$ for S2/3; $R = 0.78$, $P < 0.0001$ for S5; Fig. 3*B*,*C*). The result was algebraically identical if we first calculated the axo-dendritic overlap for each combination of PV interneuron axon and PC dendrite and somata and then averaged the results together.

To compare the 2-dimensional arrangement of the connectivity profile, we used polar plots to represent the proportion of presynaptic PV interneurons located at particular angles with respect to the PCs. This analysis also revealed that, for both somatosensory layers 2/3 and 5 PCs, the measured average polar coordinates of the connectivity were also remarkably similar to the calculated profiles, based on the axo-dendritic overlap (Fig. 3*D*,*E*). Indeed, not only was the vertical orientation conserved in the calculated maps but also the bias for S2/3 PCs to receive a higher probability of connection from PV interneurons toward the pial surface (Fig. 3*E*, left column), while S5 PCs had the opposite tendency (Fig. 3*E*, right column), was nicely recapitulated in the maps generated by the axo-dendritic overlap (Fig. 3*D*). Moreover, while the correlation between the predicted and observed connections was very high within the same layer ($R = 0.80$, $P < 0.0001$ for S2/3; $R = 0.83$, $P < 0.0001$ for S5; Fig. 3*F*), the correlation across layers was both below zero (between S2/3 predictions and S5 observations $R = -0.51$; between S5 predictions and S2/3 observations, $R = -0.12$). This indicates that differences in the spatial patterns of connectivity observed between different cortical layers can be explained solely by taking into account the differences in the morphologies of the PV axon and PC dendrites.

Overlap of Axons and Dendrites Predicts Spatial Connectivity Profiles of SOM Interneurons

We next repeated this analysis for the connectivity maps of SOM interneurons (Fig. 4). For SOM interneurons, we used measured connectivity maps from PCs from the frontal cortex layer 2/3 (Fino and Yuste 2011), but similar measurements for layer 5 PCs have not been performed. We again found a bias for SOM interneurons in a vertical column centered on the PC to be more likely to be connected (Fig. 4*A*,*F*), as presented previously for the PV interneurons (Packer and Yuste 2011). This tendency could also be visualized in the average morphology of the SOM axon (Fig. 4*B*). We used the average morphologies of reconstructed SOM axons and PC dendrites to build the calculated maps of connectivity by systematically offsetting the positions of the cell bodies of the SOM interneurons and PCs, using the coordinates of every interneuron tested from the measured input maps ($n = 1088$ pairs, all F2/3).

Similar to PV analysis, we found that the calculated connectivity maps were strikingly similar to the measured ones. Specifically, the observed connection probability at each intersomatic distance (Fig. 4*C*) was again not significantly different from the calculated axo-dendritic overlap (Fig. 4*D*; $R = 0.94$, $P < 0.0001$). In addition, the calculated and measured spatial structure of the maps was also very similar, with a highly significant correlation between the predicted (Fig. 4*E*) and the observed angular connectivity profiles (Fig. 4*F*; $R = 0.89$, $P < 0.0001$).

We conclude that the anatomical overlap between axonal arborizations of PV and SOM interneurons and dendritic arborizations of PCs was sufficient to predict the spatial patterns of connectivity, and even the difference observed across different layers, without the need of any additional mechanisms.

Differences in Targeting of Postsynaptic Compartments Between SOM and PV Interneurons

In the second part of the study, we tackled the subcellular specificity in the targeting of PC by PV and SOM neocortical interneurons (Kawaguchi and Kubota 1993, 1997; Kawaguchi 1995), seeking to reconcile it with the lack of specificity of the connectivity maps revealed by our data. Indeed, we were surprised to find that axo-dendritic overlap, albeit measured on a much larger scale than that at which synapses are formed, was able to capture many features of the interneuron connectivity we observed in our datasets. Given that basket cells, a subset of the PV interneuron population, contact the perisomatic region of their postsynaptic targets (Martin et al. 1983; Fairen et al. 1984), whereas SOM interneurons mainly target their dendrites (Kawaguchi and Kubota 1997; Wang et al. 2004), we expected to observe that these distinguishing characteristics would make axo-dendritic overlap an insufficient predictor of interneuron connectivity. In other words, how could a nonspecific application of Peters' rule predict connectivity so well (Figs 3 and 4) given the known subcellular connection specificity of these interneuron subtypes?

To explore this question, we used brain slices to perform dual whole-cell recordings from connected pairs of PV-PC ($n = 8$; from S2/3 and S5) and SOM-PC ($n = 5$; from F2/3) and reconstructed anatomically the morphologies of the interneuron axons and the PC dendrites (Supplementary Fig. S2). In these reconstructions, we then searched for synaptic contacts between known connected pairs of interneurons and PCs at the light microscope level. Using morphological reconstructions as a digital guide, we systematically searched for putative contacts among biocytin-labeled pairs of monosynaptically connected pairs of interneuron to PC (Figs 5 and 6). Viewing fixed slices with a ×100 objective, we accepted contacts as putative synaptic connections if we observed an axonal bouton of an interneuron within 1 μm of a PC dendrite or soma.

Using this approach, we tabulated the position of putative contacts from PV-PC and SOM-PC pairs. On average, each PV-PC pair had 4 putative contacts, distributed along the soma and dendrites (Fig. 5*A*). SOM-PC pairs had an average of 9 putative contacts, widely distributed along the dendritic tree of the PC (Fig. 6*A*). As previously described (Kawaguchi and Kubota 1997; Wang et al. 2002; Di Cristo et al. 2004), connections were significantly closer to the postsynaptic cell body in PV to PC pairs compared with the ones in SOM to PC pairs (Table 1). Therefore, the spatial location of the putative contacts of neocortical SOM and PV axons in our sample resembled the ones confirmed with ultrastructural techniques (Kawaguchi and Kubota 1997; Wang et al. 2002).

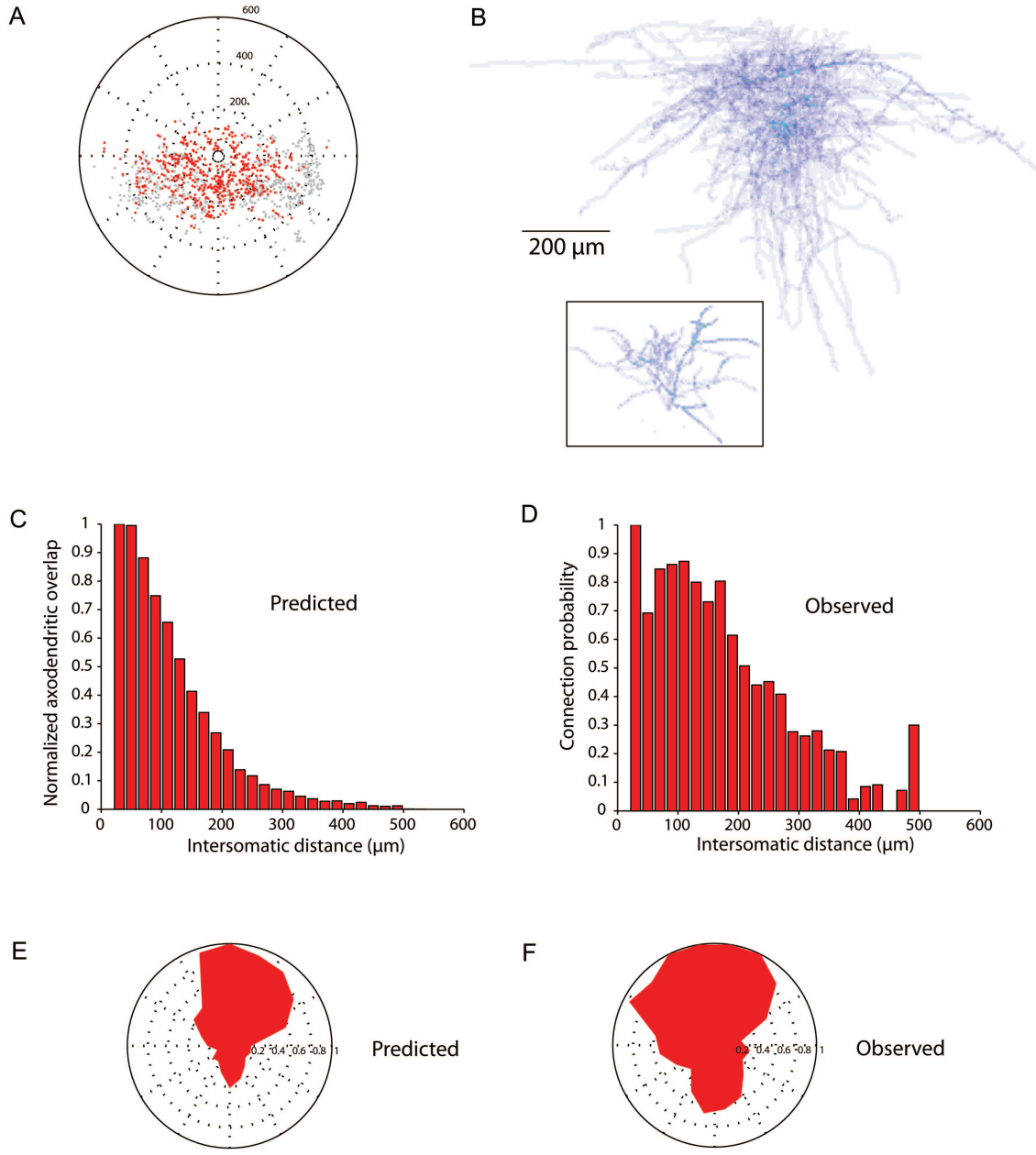

Figure 4. Axo-dendritic overlap can predict the spatial patterns of SOM connectivity. (*A*) Position of the connected (red) and unconnected (gray) SOM interneurons plotted relative to the recorded PC (center). (*B*) Average density of 5 frontal cortex layer 2/3 SOM interneuron axons (top) and 4 frontal cortex layer 2/3 PC apical dendrites (black box) was multiplied to produce a measure of axo-dendritic overlap between axons of SOM interneurons and apical dendrites of PCs. (*C*) The predicted probability of connection versus intersomatic distance between the SOM interneuron and the PC based on axo-dendritic overlap. (*D*) Observed probability of connection versus intersomatic distance, calculated as the number of connected interneurons out of the total number of connected and unconnected interneurons (presented in Fino and Yuste (2011) and slightly different than the expected probability since the calculated probability included false positives in the denominator). (*E–F*) Predicted and observed probabilities of connection versus angle between the SOM interneuron and the PC (center).

Laminar Targeting Can Explain Postsynaptic Targeting by PV and SOM Interneurons

We then examined whether the axons of interneurons could have contacted the postsynaptic cell's processes by chance alone. Using the database of putative contacts, we explored whether Peter's rule could explain their spatial patterns by comparing their spatial distribution with that of available postsynaptic membrane of the PC. To do so, we analyzed the morphology of the reconstructed PCs and calculated the surface area of the soma and dendrites (see Materials and Methods). We then computed a histogram of the surface area versus distance from the postsynaptic soma, similar to a Sholl analysis, except using the surface area (rather than the branch number), as the measured variable, since it is the area, rather than the branch number, that applies in Peter's rule. We found that the histograms of contacts and surface area versus distance from the postsynaptic soma were not significantly different for PV to PC pairs (Fig. 5*C*; Wilcoxon matched-pairs signed-ranks test, $P > 0.05$) or for SOM to PC pairs (Fig. 6*C*; Wilcoxon test, $P > 0.05$). While there was a slight bias to find more connections on the soma in PV to PC pairs than in SOM to PC pairs (Figs 5*C* vs. 6*C*; first bin in each histogram), there

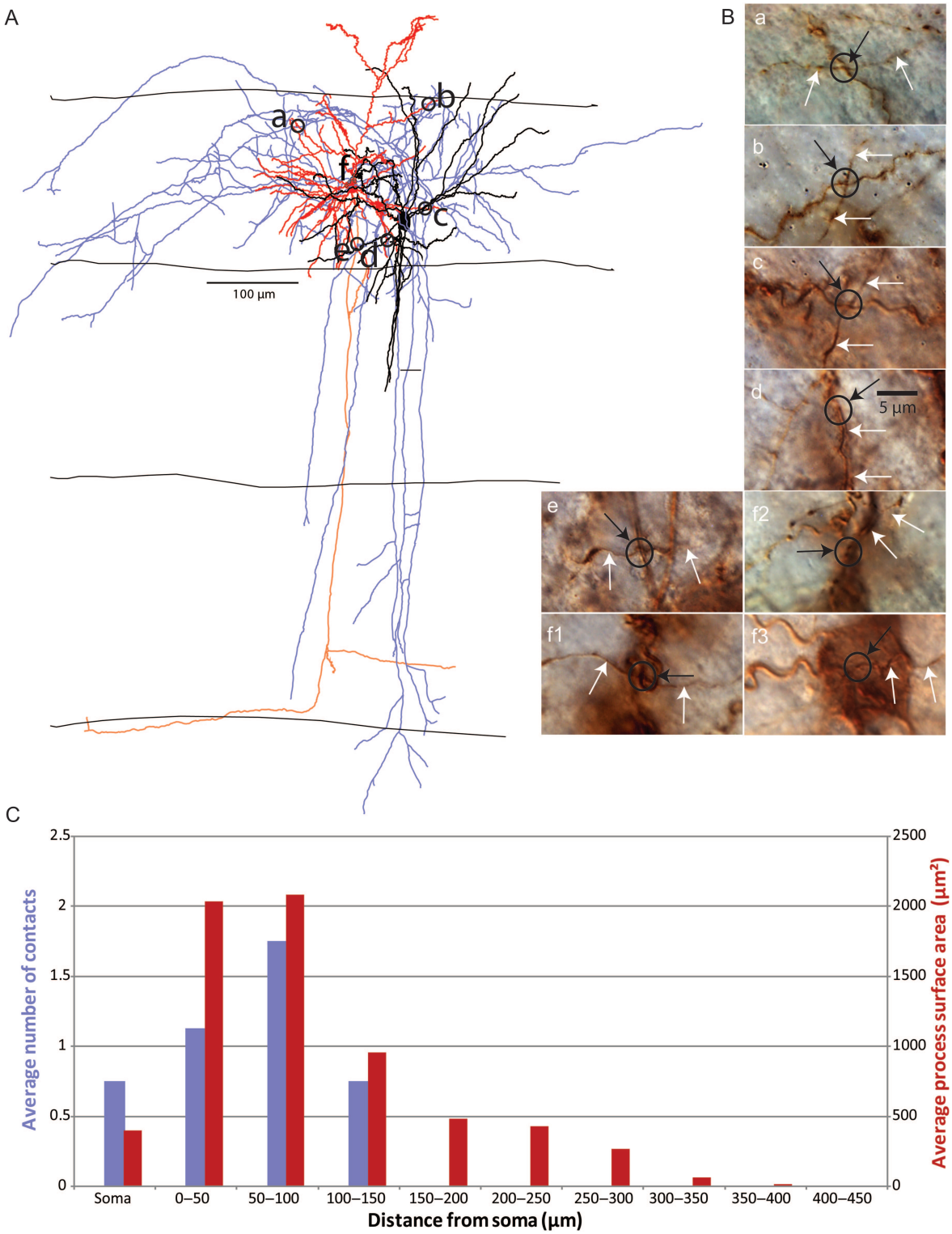

Figure 5. Position of synaptic connections from PV interneurons to PCs. (*A*) Anatomical reconstruction of a PV-PC pair with location of contacts from PV axon to PC dendrite or soma. PC soma and dendrites in red, axon in orange. PV soma and dendrites in black, axon in blue. Layer boundaries drawn. (*B*) Photomicrographs of contacts from biocytin-labeled neurons (black circle surrounds contact, white arrow indicates PV axon, black arrow points to contact, label corresponds to location on anatomical reconstruction). (*C*) Average number of connections (purple bars) and average process surface area in hundreds of μm^2 (red bars) versus distance from PC soma. First bin includes only the soma.

were still somatic connections from the SOM interneurons, in agreement with electron microscopy evidence (see Discussion).

Our data therefore demonstrated that, on the one hand, PV and SOM cells make contact in different and selective parts of the PC (Table 1), yet that these contacts are made apparently

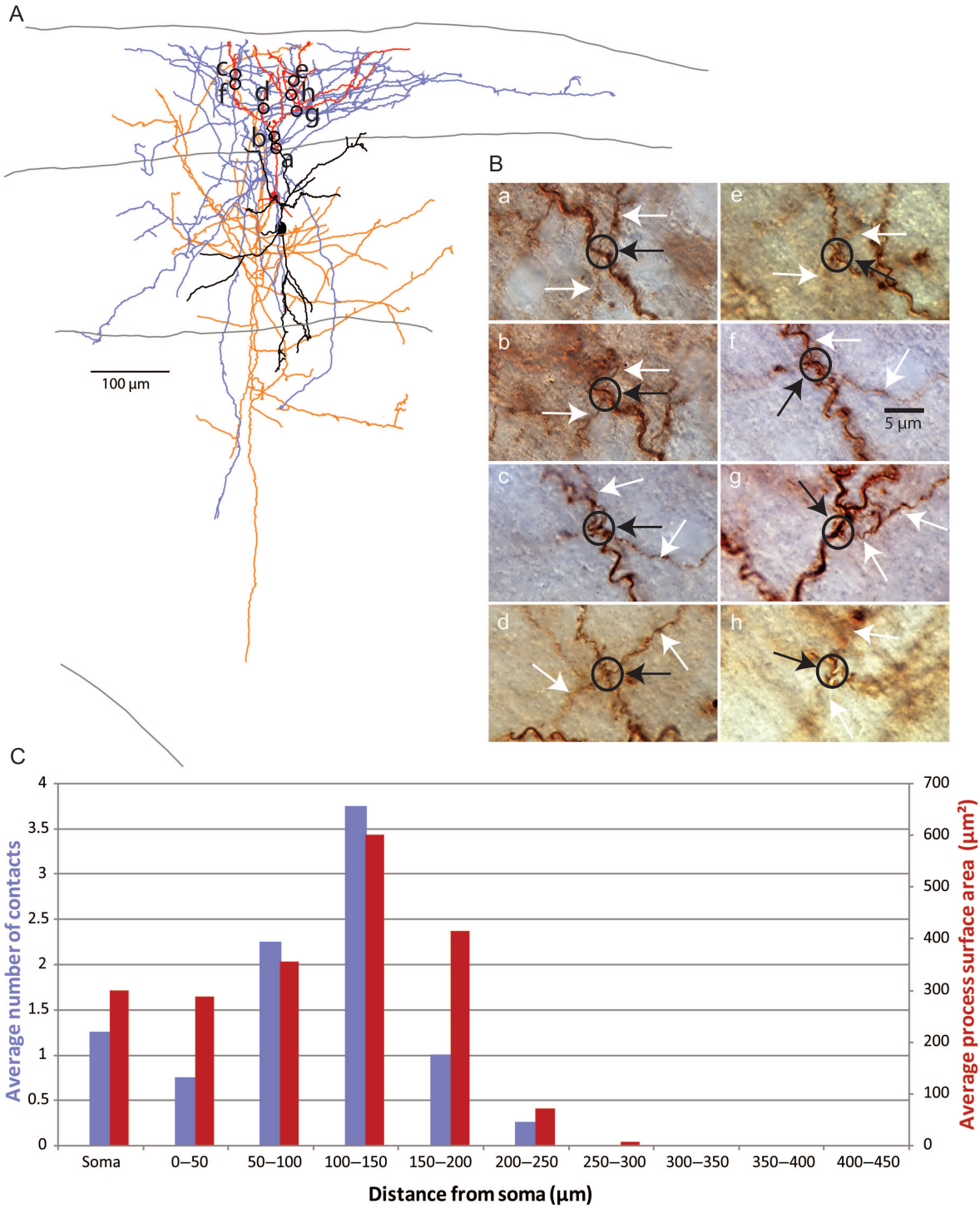

Figure 6. Position of synaptic connections from SOM interneurons to PCs. (*A*) Anatomical reconstruction of a SOM-PC pair with location of contacts from SOM axon to PC dendrite. PC soma and dendrites in red, axon in orange. SOM cell soma and dendrites in black, axon in blue. Pia, layer 2/3 and layer 4 boundaries, and white matter drawn. (*B*) Photomicrographs of contacts from reconstruction (black circle surrounds contacts, white arrow indicates SOM cell axon, black arrow points to connection, label corresponds to location on anatomical reconstruction). (*C*) Average number of connections (purple bars) and average process surface area in hundreds of μm^2 (red bars) versus distance from PC soma. First bin includes only the soma. Also note that the small difference in the distribution of layer 2/3 PC dendritic surface area compared with Figure 5*C* is due to the random selection of PCs further from the pial surface here.

in directly proportion to the area of overlap, as if they were nonselective (Figs 5 and 6). To reconcile these results, we explored whether the known differences in laminar targeting of PV and SOM cells could explain the subcellular specificity in connections onto PC cells. For this purpose, we measured the length of interneuron axon of each type of cell that is present in layers 1 and 2/3 (Table 2). While there was no statistical difference between the length of PV interneuron axon and the length of SOM interneuron axon in layer 2/3, there was significantly less PV interneuron axon than SOM interneuron axon in layer 1. This difference was even more striking when calculating the ratio of axon length in layer 2/3 to

axon length in layer 1 for each cell type (Table 2). Indeed, we found over a 100-fold difference in this ratio between the PV and SOM populations, implying a stark contrast between the laminar targets of the axons of these 2 interneuron subtypes. Thus, since layer 1 lacks PC somata and proximal dendrites, it is possible that the subcellular specificity of interneuron PC connections arises from laminar targeting by the interneuron axon (Fig. 7). When the axon invades its chosen layer, it could then make promiscuous and nonspecific contacts with whichever postsynaptic targets it finds in that layer—mostly somata and proximal dendrites of PCs in layer 2/3, and solely distal dendrites from PCs in layer 1.

Discussion

In this study, we sought to understand the potential mechanisms by which SOM and PV interneurons innervate their PC targets very densely and to reconcile the subcellular target specificity of PV and SOM neocortical interneurons with their unspecific innervation of PCs. We performed this study in developing somatosensory and frontal neocortex of juvenile mice and analyzed a database of inhibitory connectivity (Fino and Yuste 2011; Packer and Yuste 2011) and a morphological database of PV, SOM, and PC neurons, to examine anatomical explanations for how interneurons form connections in the neocortex. In the first part of the study, we performed a macroscopic analysis, finding that Peters' rule, which states that axo-dendritic overlap determines synaptic connectivity, can predict the spatial features of SOM and PV inputs to PCs in the neocortex, and, specifically, the distance dependency and the polar coordinates of the location of connected cells. In the second part of the study, carried out at a finer scale, we found that Peters' rule can also explain the position of contacts from interneurons onto a postsynaptic cell's compartment, because these contacts are located in proportion to the postsynaptic membrane area. Thus, laminar targeting by interneuron axons may provide the most parsimonious explanation for the subcellular specificity observed in the position of contacts on PCs.

We conclude that an unspecific explanation based on Peters' rule could account for the connectivity observed from SOM and PV to PCs at these early developmental stages, during the second to third postnatal weeks. Apparently, details such as the exact position of axonal boutons or the fine targeting on postsynaptic processes are not necessary to accurately recapitulate the correct connectivity profile, consistent with the idea that these SOM and PV axons connect in an unspecific manner with whatever postsynaptic structure they encounter in their target layer.

Table 1
Contacts between interneurons and PCs determined at the light microscope level

	PV ($n = 8$)	SOM ($n = 4$)	Significance
Number	4.4 ± 1.0	9.3 ± 0.5	*
Distance (direct, μm)	55 ± 7	95 ± 9	***
Distance (along dendrite, μm)	70 ± 10	123 ± 12	**
Branch order	3.6 ± 0.5	4.5 ± 0.5	ns

ns, not significant; *$P < 0.05$, **$P < 0.01$, ***$P < 0.001$, Mann–Whitney test.

Table 2
Length of axon from interneurons in layer 2/3 versus layer 1

	PV ($n = 7$)	SOM ($n = 4$)	Significance
Length of axon in layer 2/3 (μm)	10 485 ± 2414	8501 ± 2289	ns
Length of axon in layer 1 (μm)	198 ± 81	6997 ± 1126	**
Ratio of length of axon in layer 2/3 versus layer 1	200 ± 110	1.4 ± 0.5	**

ns, not significant; *$P < 0.05$, **$P < 0.01$.

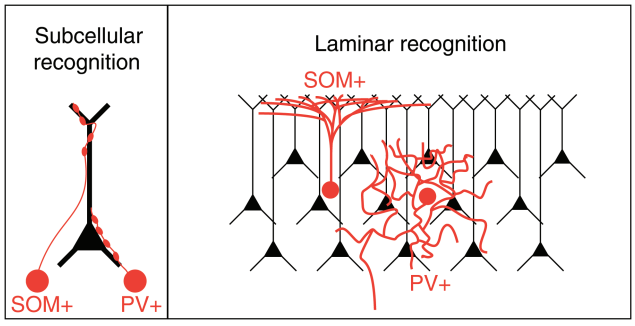

Figure 7. Models of interneuron connectivity. (*A*) Molecular recognition model: SOM interneurons specifically recognize and target distal dendritic trees of PCs, whereas PV axons target somatic compartments. (*B*) Laminar model: By projecting to layer 1, where only distal dendrites are present, SOM interneurons avoid contacting somata and proximal dendrites of PCs. PV interneurons, on the other hand, project to layer 2/3 and thus avoid contacting distal dendrites.

Intralaminar Mechanism of Interneuron Connectivity

The first goal of our study focused on understanding how the promiscuous connectivity of SOM and PV interneurons to PC could emerge (Fino and Yuste 2011; Packer and Yuste 2011). Using the average morphologies of representative SOM and PV axons and PC dendrites, and positioning them in the exact somatic locations of the SOM and PV interneurons found in the connectivity maps, we used numerical simulations to build calculated connectivity maps that closely resemble the measured ones, in both the distribution of the connection probability and the spatial organization of the PC targets (Figs 3 and 4). Thus, the spatial pattern of connectivity between interneurons and PCs is consistent with Peters' rule (Peters and Feldman 1976). This is surprising because, at least for excitatory circuits, Peters' rule is often violated (Stepanyants et al. 2002; Brown and Hestrin 2009; Petreanu et al. 2009; Mishchenko et al. 2010; but see Shepherd et al. 2005). Our finding that Peters' rule is sufficient to explain the spatial distribution of connectivity from PV and SOM interneurons does not mean that all aspects of their connectivity are unspecific. As we argue below, at the macroscopic level, there are clear patterns of interlaminar projections of interneurons (Katzel et al. 2011), as can be observed in our reconstructions, where certain layers appear to be specifically targeted (Fig. 2). At the microscopic level, there is also clear evidence for extreme specificity for some connections, such as those made by chandelier cells (Somogyi 1977).

Our results nevertheless reveal a lack of specificity in the local connections made by PV and SOM of interneurons, indicating that these interneurons do not avoid particular postsynaptic cells, but connect with whomever they encounter. If the

function of inhibition is to achieve a balance with excitation, then this lack of anatomical specificity may provide the underlying hardware. In agreement with this, recent experiments in vivo have demonstrated the lack of selectivity in both interneuron inputs and outputs. At the anatomical level, interneurons appear to receive inputs from excitatory neurons with a range of preferred orientations (Bock et al. 2011). Functionally, neocortical interneurons are broadly tuned to orientation (Sohya et al. 2007; Niell and Stryker 2008; Kerlin et al. 2010; Zariwala et al. 2011; but see also Runyan et al. 2010). Finally, another type of interneuron, the neurogliaform cells, can release GABA in the neuropil in a nonsynaptic fashion (Olah et al. 2009).

Mechanism for Selection of Postsynaptic Compartments

The second goal of our study was to reconcile the apparent lack of specificity in the connectivity maps of interneurons with their clear selectivity in contacting different postsynaptic cellular compartments. Indeed, electron microscope studies have shown that different interneurons subtypes have subcellular specificity in their targeting (Somogyi et al. 1998). Basket cells, which are PV-positive, generally target the soma or somatic region with ~30% of their boutons (Kisvárday 1992), while dendrite-targeting cells, most of which are likely to be SOM-positive, only contact the soma with 7% of their boutons (Wang et al. 2002). Such preferential targeting seems to violate Peters' rule because PV interneuron axons course through areas in which nonperisomatic dendrites of PCs reside, while SOM interneuron axons surely must pass near PC somas.

We explored this question quantitatively using anatomical reconstructions of connected pairs of SOM-PCs and PV-PCs, locating potential synaptic contacts between pairs of interneurons and PCs at the light microscopy level. This method has been shown in the past to correspond well, and sometimes perfectly, to ultrastructural identification of contacts (DeFelipe and Fairen 1982; Reyes et al. 1998; Tamas et al. 2002; Kalisman et al. 2005; Tanaka et al. 2011) and indeed, although we did not perform ultrastructural analysis of our data, the pattern of putative contacts that we find differ between SOM and PV interneurons, in good agreement with the ultrastructural literature (DeFelipe and Fairen 1982; Cobb et al. 1997; Tamas et al. 1997, 2002; Wang et al. 2002; Tanaka et al. 2011). But, surprisingly, we find at the same time that the position of the putative contacts closely matches the availability of postsynaptic membrane (Figs 5 and 6). Although there is a slight bias for PV interneurons to make connections more closely to the postsynaptic soma, most of their putative contacts of PV-PC and SOM-PC statistically match the available surface area of the PC, as if there were no selectivity in the interneuron innervation. In addition, we quantify results that demonstrate that SOM interneuron axons arborize much more in layer 1 than PV interneuron axons. Therefore, the innervation pattern closely corresponds to what would be expected if interneurons were to send axons to a specific layer and then simply contact their postsynaptic targets wherever they hit them in the tissue.

A Laminar Model for the Formation of Inhibitory Connections in Neocortex

How can one reconcile the selectivity in innervating specific somato-dendritic compartments with their local unspecific innervation of PCs? We would argue that the preference for SOM interneurons to contact distal dendrites could arise quite naturally from the fact that they mostly project to layer 1, which lacks PC somata and proximal dendrites (Fig. 7; "Laminar" model; Table 2). Similarly, PV interneurons mostly contact PCs within the same layer, avoiding layer 1 and, by doing so, project by default to layers that are more enriched with PC somata and proximal dendrites. In our view, the subcellular specificity in targeting would then, at least partly, arise from the laminar specificity in the projections, without needing additional molecular mechanisms that label proximal and distal dendritic compartments in PCs (Fig. 7; "Subcellular Recognition" model). One could argue that perhaps the targeting of particular layers could result from axons searching for subcellular-specific cues. For example, SOM interneurons could be specifically attracted to a molecular cue present on on distal dendrites and because of this they would therefore target layer 1. But if this were the case, one would expect more selectivity in the position of SOM contacts, which, besides contacting distal dendrites, are also found on proximal dendrites or even somata (Fig. 6). Similarly, in our data, and in ultrastructural reconstructions from other groups (DeFelipe and Fairen 1982; Cobb et al. 1997; Tamas et al. 2002; Tanaka et al. 2011), most of the PV contacts are actually not on the soma, and this apparent "sloppiness" in targeting is difficult to reconcile with a scenario where the location of these synapses would be strictly dictated by the presence of a somatic molecular cue. Indeed, there is evidence that GABAergic synapses can develop at pre-existing axon-dendrite crossings without the need for additional protrusions being formed by either the axons or dendrites (Wierenga et al. 2008). Moreover, in agreement with this apparent lack of selectivity, visual inspection of the potential contacts in our samples reveals that the SOM and PV axons tend to cross the dendrites with orthogonal "en passant" trajectories, as if they encountered them by chance and then continued, rather than as if they were specifically attracted to the dendrites (Figs 5 and 6; insets).

Our results do not rule out the existence of specific subcellular targeting mechanisms, but indicate that they are not strictly necessary to explain the selectivity of neocortical PV and SOM interneurons. Previous studies have argued that specific subcellular molecular recognition mechanisms must be present genetically, since organotypic cultures preserve the somato-dendritic differences in innervation between PV and SOM interneurons (Di Cristo et al. 2004; Chattopadhyaya et al. 2007). However, organotypic cultures also preserve laminar structures and perhaps this specific subcellular innervation is also a byproduct of earlier laminar specificity. Nevertheless, there are cases where molecular recognition of subcellular compartments must be present in interneuron innervation. For example, chandelier cells, which are developmentally related to PV cells (Xu et al. 2008), must rely on very specific subcellular recognition signals since they project exclusively to axon initial segments, without mistakes (Somogyi 1977; Inan, M. et al. in preparation). We recognize that our sample of PV-PC reconstructions was not extensive and that perhaps a larger database could demonstrate statistically a stronger bias for targeting somatic membranes by PV interneurons.

In addition, it is important to recognize that our results (and those of Wierenga et al. (2008)) apply solely to relatively early developmental stages, and different results, demonstrating stronger subcellular selectivity in PV or SOM targeting may be found in adult preparations. The earlier connectivity pattern

could be less specific than the mature one, particularly if there is developmental pruning or selective addition of new connections. Indeed, the number of PV interneuron boutons forming synapses onto somata increases throughout development (Chattopadhyaya et al. 2007). Because we have only examined juvenile animals (P11–17), it is possible that our analysis reveals only the initial mechanisms of the interneuron connectivity program, with more specific pruning or targeting mechanisms coming online as the cortex matures. Nevertheless, in our 2-photon photostimulation mapping, we observed a dense inhibitory connectivity in adult animals, similar to the one observed in juvenile mice (Fino and Yuste 2011; Packer and Yuste 2011). While anatomical data demonstrate that basket cells, true to their namesake, occasinally target and wrap around postsynaptic somata (DeFelipe and Fairen 1982; Martin et al. 1983; Fairen et al. 1984), it is also possible that, when basket cell axons reach somata, they make numerous contacts along somatic membranes simply because they encounter large postsynaptic surface areas when forced to skirt somatic boundaries.

In closing, to reconcile results demonstrating the apparent lack of specificity in the interneuronal output connections (e.g. this study, Wierenga et al. 2008), with studies demonstrating clear specificity (e.g. Somogyi 1977; Ango et al. 2004), one could suggest that the innervation pattern of interneurons results from a combination of mechanisms, some unspecific, such as the intralaminar spatial connectivity patterns determined by axo-dendritic overlap as in Peters' rule, and others specific, such as laminar and, in some cases, also subcellular targeting. Based on our laminar model (Fig. 7), we propose that, like in hippocampus, where the strict lamination generates different laminar positions for different subcellular compartments of PCs (Buhl et al. 1994), neocortical interneurons could, at least partly, achieve specific subcellular targeting simply by projecting to the appropriate layers and then connecting promiscuously with whatever postsynaptic membrane they encounter. This could ensure both a selective innervation of the appropriate subcellular compartment and the widespread connections to all potential PC targets, thus enabling these apparently contradictory missions that require opposite extremes of specificity. The common strategy used by the neocortex and hippocampus further reveals the deep evolutionary relation between these structures, highlighting the usefulness of comparative approaches to understand neuronal circuits.

Supplementary Material

Supplementary material can be found at: http://www.cercor.oxfordjournals.org/.

Notes

We thank Y. Shin for anatomical reconstructions, M. Atiya for initial analysis, M. Dar, T. Sippy, A. Woodruff, and other members of the laboratory for help and comments and anonymous reviewers for their suggestions. Supported by the Kavli Institute for Brain Science, the Keck Foundation and the National Eye Institute. *Conflict of Interest*: None declared.

References

Ango F, di Cristo G, Higashiyama H, Bennett V, Wu P, Huang ZJ. 2004. Ankyrin-based subcellular gradient of neurofascin, an immunoglobulin family protein, directs GABAergic innervation at purkinje axon initial segment. Cell. 119:257–272.

Ango F, Wu C, Van der Want JJ, Wu P, Schachner M, Huang ZJ. 2008. Bergmann glia and the recognition molecule CHL1 organize GABAergic axons and direct innervation of Purkinje cell dendrites. PLoS Biol. 6:e103.

Ascoli GA, Alonso-Nanclares L, Anderson SA, Barrionuevo G, Benavides-Piccione R, Burkhalter A, Buzsaki G, Cauli B, Defelipe J, Fairen A et al. 2008. Petilla terminology: nomenclature of features of GABAergic interneurons of the cerebral cortex. Nat Rev Neurosci. 9:557–568.

Berens P. 2009. CircStat: a MATLAB toolbox for circular statistics. J Stat Softw. 31:1–21.

Bock DD, Lee WC, Kerlin AM, Andermann ML, Hood G, Wetzel AW, Yurgenson S, Soucy ER, Kim HS, Reid RC. 2011. Network anatomy and in vivo physiology of visual cortical neurons. Nature. 471:177–182.

Brown SP, Hestrin S. 2009. Intracortical circuits of pyramidal neurons reflect their long-range axonal targets. Nature. 457:1133–1136.

Buhl EH, Halasy K, Somogyi P. 1994. Diverse sources of hippocampal unitary inhibitory postynaptic potentials and the number of synaptic release sites. Nature. 368:823–828.

Buzsaki G, Chrobak JJ. 1995. Temporal structure in spatially organized neuronal ensembles: a role for interneuron networks. Curr Opin Neurobiol. 5:504–510.

Chattopadhyaya B, Di Cristo G, Higashiyama G, Knott GW, Kuhlman SJ, Welker E, Huang ZJ. 2004 Experience and activity-dependent maturation of perisomatic GABAergic innervation in primary visual cortex during a postnatal critical period. J Neurosci. 24: 9598–9611.

Chattopadhyaya B, Di Cristo G, Wu CZ, Knott G, Kuhlman S, Fu Y, Palmiter RD, Huang ZJ. 2007. GAD67-mediated GABA synthesis and signaling regulate inhibitory synaptic innervation in the visual cortex. Neuron. 54:889–903.

Cobb SR, Halasy K, Vida I, Nyiri G, Tamas G, Buhl EH, Somogyi P. 1997. Synaptic effects of identified interneurons innervating both interneurons and pyramidal cells in the rat hippocampus. Neuroscience. 79:629–648.

Cuntz H, Forstner F, Borst A, Hausser M. 2010. One rule to grow them all: a general theory of neuronal branching and its practical application. PLoS Comput Biol. 6(8): e1000877.

DeFelipe J, Fairen A. 1982. A type of basket cell in superficial layers of the cat visual cortex. A Golgi-electron microscope study. Brain Res. 244:9–16.

Di Cristo G, Wu C, Chattopadhyaya B, Ango F, Knott G, Welker E, Svoboda K, Huang ZJ. 2004. Subcellular domain-restricted GABAergic innervation in primary visual cortex in the absence of sensory and thalamic inputs. Nature Neurosci. 7:1184–1186.

Fairen A, De Felipe J, Regidor J. 1984. Nonpyramidal neurons. In Peters A, Jones EG editors. Cerebral cortex. New York: Plenum. p. 201–253.

Fino E, Araya R, Peterka DS, Salierno M, Etchenique R, Yuste R. 2009. RuBi-Glutamate: two-photon and visible-light photoactivation of neurons and dendritic spines. Front Neural Circuits. 3:2.

Fino E, Yuste R. 2011. Dense inhibitory connectivity in neocortex. Neuron. 69:1188–1203.

Huang ZJ, Di Cristo G, Ango F. 2007. Development of GABA innervation in the cerebral and cerebellar cortices. Nature Rev Neurosci. 8:673–686.

Kalisman N, Silberberg G, Markram H. 2005. The neocortical microcircuit as a tabula rasa. Proc Natl Acad Sci USA. 102:880–885.

Kapfer C, Glickfeld LL, Atallah BV, Scanziani M. 2007. Supralinear increase of recurrent inhibition during sparse activity in the somatosensory cortex. Nature Neurosci. 10:743–753.

Katzel D, Zemelman BV, Buetfering C, Wolfel M, Miesenbock G. 2011. The columnar and laminar organization of inhibitory connections to neocortical excitatory cells. Nat Neurosci. 14:100–107.

Kawaguchi Y. 1995. Physiological subgroups of nonpyramidal cells with specific morphological characteristics in layer II/III of rat frontal cortex. J Neurosci. 15:2638–2655.

Kawaguchi Y, Kubota Y. 1993. Correlation of physiological subgroupings of nonpyramidal cells with parvalbumin- and calbindinD28k-immunoreactive neurons in layer V of rat frontal cortex. J Neurophysiol. 70:387–396.
Kawaguchi Y, Kubota Y. 1997. GABAergic cell subtypes and their synaptic connections in rat frontal cortex. Cereb Cortex. 7:476–486.
Kerlin AM, Andermann ML, Berezovskii VK, Reid RC. 2010. Broadly tuned response properties of diverse inhibitory neuron subtypes in mouse visual cortex. Neuron. 67:858–871.
Kisvárday ZF. 1992. Gaba in the retina and central visual system. In: Progress in Brain Research. Chapter 18, Vol. 90. Elsevier. p. 385–405. http://dx.doi.org/10.1016/S0079-6123(08)63623-7.
Lewis DA, Fish KN, Arion D, Gonzalez-Burgos G. 2011. Perisomatic inhibition and cortical circuit dysfunction in schizophrenia. Curr Opin Neurobiol 21:866–872.
Martin KA, Somogyi P, Whitteridge D. 1983. Physiological and morphological properties of identified basket cells in the cat's visual cortex. Exp Brain Res. 50:193–200.
McGarry LM, Packer AM, Fino E, Nikolenko V, Sippy T, Yuste R. 2010. Quantitative classification of somatostatin-positive neocortical interneurons identifies three interneuron subtypes. Front Neural Circuits. 4:12.
Mishchenko Y, Hu T, Spacek J, Mendenhall J, Harris KM, Chklovskii DB. 2010. Ultrastructural analysis of hippocampal neuropil from the connectomics perspective. Neuron. 67:1009–1020.
Monyer H, Markram H. 2004. Interneuron diversity series: molecular and genetic tools to study GABAergic interneuron diversity and function. Trends Neurosci. 27:90–97.
Niell CM, Stryker MP. 2008. Highly selective receptive fields in mouse visual cortex. J Neurosci. 28:7520–7536.
Nikolenko V, Poskanzer KE, Yuste R. 2007. Two-photon photostimulation and imaging of neural circuits. Nat Methods. 4:943–950.
Olah S, Fule M, Komlosi G, Varga C, Baldi R, Barzo P, Tamas G. 2009. Regulation of cortical microcircuits by unitary GABA-mediated volume transmission. Nature. 461:1278–1281.
Oliva AA, Jr, Jiang M, Lam T, Smith KL, Swann JW. 2000. Novel hippocampal interneuronal subtypes identified using transgenic mice that express green fluorescent protein in GABAergic interneurons. J Neurosci. 20:3354–3368.
Packer AM, Yuste R. 2011. Dense, unspecific connectivity of neocortical parvalbumin-positive interneurons: a canonical microcircuit for inhibition? J Neurosci. 31:13260–13271.
Peters A, Feldman ML. 1976. The projection of the lateral geniculate nucleus to area 17 of the rat cerebral cortex. I. General description. J Neurocytol. 5:63–84.
Peters A, Paley SL, Webster HdF. 1976. The fine structure of the nervous system. Philadelphia: Saunders.
Petreanu L, Mao T, Sternson SM, Svoboda K. 2009. The subcellular organization of neocortical excitatory connections. Nature. 457:1142–1145.
Prince DA, Wilder BJ. 1967. Control mechanisms in cortical epileptogenic foci. "Surround" inhibition. Arch Neurol. 16:194–202.
Reyes A, Lujan R, Rozov A, Burnashev N, Somogyi P, Sakmann B. 1998. Target-cell-specific facilitation and depression in neocortical circuits. Nat Neurosci. 1:279–285.
Runyan CA, Schummers J, Van Wart A, Kuhlman SJ, Wilson NR, Huang ZJ, Sur M. 2010. Response features of parvalbumin-expressing interneurons suggest precise roles for subtypes of inhibition in visual cortex. Neuron. 67:847–857.
Shepherd GM, Stepanyants A, Bureau I, Chklovskii D, Svoboda K. 2005. Geometric and functional organization of cortical circuits. Nat Neurosci. 8:782–790.
Sohya K, Kameyama K, Yanagawa Y, Obata K, Tsumoto T. 2007. GABAergic neurons are less selective to stimulus orientation than excitatory neurons in layer II/III of visual cortex, as revealed by in vivo functional Ca2+ imaging in transgenic mice. J Neurosci. 27:2145–2149.
Somogyi P. 1977. A specific 'axo-axonal' interneuron in the visual cortex of the rat. Brain Res. 136:345–350.
Somogyi P, Tamas G, Lujan R, Buhl E. 1998. Salient features of synaptic organisation in the cerebral cortex. Brain Res Brain Res Rev. 26:113–135.
Stepanyants A, Hof PR, Chklovskii DB. 2002. Geometry and structural plasticity of synaptic connectivity. Neuron. 34:275–288.
Tamas G, Buhl EH, Somogyi P. 1997. Fast IPSPs elicited via multiple synaptic release sites by different types of GABAergic neurone in the cat visual cortex. J Physiol. 500:715–738.
Tamas G, Szabadics J, Somogyi P. 2002. Cell type- and subcellular position-dependent summation of unitary postsynaptic potentials in neocortical neurons. J Neurosci. 22:740–747.
Tanaka YH, Tanaka YR, Fujiyama F, Furuta T, Yanagawa Y, Kaneko T. 2011. Local connections of layer 5 GABAergic interneurons to corticospinal neurons. Front Neural Circuits. 5:12.
Wang Y, Gupta A, Toledo-Rodriguez M, Wu CZ, Markram H. 2002. Anatomical, physiological, molecular and circuit properties of nest basket cells in the developing somatosensory cortex. Cereb Cortex. 12:395–410.
Wang Y, Toledo-Rodriguez M, Gupta A, Wu C, Silberberg G, Luo J, Markram H. 2004. Anatomical, physiological and molecular properties of Martinotti cells in the somatosensory cortex of the juvenile rat. J Physiol. 561:65–90.
Wierenga C, Becker N, Bonhoeffer T. 2008. GABAergic synapses are formed without the involvement of dendritic protrusions. Nat Neurosci. 11:1044–1052.
Xu Q, Tam M, Anderson SA. 2008. Fate mapping Nkx2.1-lineage cells in the mouse telencephalon. J Comp Neurol. 506:16–29.
Zariwala HA, Madisen L, Ahrens KF, Bernard A, Lein ES, Jones AR, Zeng H. 2011. Visual tuning properties of genetically identified layer 2/3 neuronal types in the primary visual cortex of cre-transgenic mice. Front Syst Neurosci. 4:162.